

Nondegenerate Four-Wave Mixing in a Dual Mode Injection Locked Quantum Dot Laser

Frédéric Grillot^a, Cheng Wang^{a,b}, Ivan A. Aldaya-Garde^{a,c}, Christophe Gosset^a, Thomas Batte^b, Etienne Decerle^d, and Jacky Even^b

^aTelecom ParisTech, Ecole Nationale Supérieure des Télécommunications, CNRS LTCI, 46 rue Barrault, 75634 Paris Cedex 13, France

^bUniversité Européenne de Bretagne, INSA, CNRS FOTON, 20 avenue des Buttes de Coësmes, 35708 Rennes Cedex 7, France

^cInstituto Tecnológico y de Estudios Superiores de Monterrey, Monterrey, Mexico

^dYenista Optics, 4, rue Louis de Broglie, 22300 Lannion Cedex, France

*grillot@telecom-paristech.fr

ABSTRACT

Nondegenerate four-wave mixing (NDFWM) in semiconductor gain media is a promising source for wavelength conversion in the wavelength division multiplexed (WDM) systems and for fiber dispersion compensation in long distance fiber links. In contrast to bulk and quantum well (QW) semiconductors, the quantum dot (QD) gain medium is favorable for enhancing the performance of the FWM because of the wide gain spectrum, large nonlinear effect as well as ultrafast carrier dynamics. Especially, the destructive interference can be eliminated due to the reduced linewidth enhancement factor (LEF) for obtaining high efficiency in the wavelength up-conversion. This work reports the NDFWM generation in a dual-mode injection-locked QD Fabry-Perot (FP) laser. The device has a wide gain spectrum with a full width at half maximum of 81 nm, and a peak net modal gain of 14.4 cm⁻¹. The laser exhibits two lasing peaks induced by Rabi oscillation, which provides the possibility for efficient FWM generation. Employing the dual-mode injection-locking scheme, an efficient NDFWM is achieved up to a detuning range of 1.7 THz with a weak injection ratio of 0.44. The highest measured values for both the normalized conversion efficiency (NCE) and the side-mode suppression ratio (SMSR) with respect to the converted signal respectively are -17 dB and 20.3 dB at the detuning 110 GHz.

Keywords: quantum dot laser, optical injection locking, four-wave mixing

1. INTRODUCTION

Optical wavelength conversion plays an important role in wavelength division multiplexed (WDM) systems. NDFWM in semiconductor gain media is a desirable technique for wavelength conversion due to its ultrafast nature and transparency to the modulation format of the signals [1], [2]. In addition, since the converted signal is the phase-conjugate replica of the input signal, it also provides the possibility for fiber dispersion compensation in long distance transmission systems [3], [4]. NDFWM in semiconductor optical amplifiers (SOAs) and distributed feedback (DFB) lasers have been extensively studied and much effort has been devoted to enhance the conversion efficiency (the ratio of the output-converted signal power to the input-signal power) and the optical signal-to-noise ratio [5]-[9]. Generally, the SOA has a larger linear gain, which provides high conversion efficiency, whereas it also generates additional amplified spontaneous emission noise. In this way, there is an optimum linear gain for the maximum conversion efficiency to noise ratio [5], while a compromise on the pump-wave power is also required to obtain a better performance [6]. In DFB lasers, the lasing mode itself is used as a pump wave, and the NDFWM is enhanced by the cavity resonance. A higher conversion efficiency associated with a lower noise level can be achieved from a laser with a long cavity and a small grating coupling coefficient. A high lasing power is also favorable for obtaining higher conversion efficiency [7]-[9]. As for the nonlinear gain medium, in contrast to the QW material, QDs offer various advantages such as a wider gain spectrum [10], ultrafast carrier dynamics [11], higher nonlinear gain effect and thus a larger three-order nonlinear susceptibility [9], [12],

[13]. In addition, due to the reduced (LEF), QDs have the possibility of eliminating destructive interference among the nonlinear processes and also offer an enhanced efficiency in the wavelength up-conversion [14], [15]. In order to improve the dynamical performance of semiconductor lasers, the so-called optical injection-locking technique has been widely used to reduce the spectral linewidth, frequency chirp as well as to suppress relative intensity noise and nonlinear distortion [16]-[18]. In particular, it has been reported that the LEF value can be reduced under strong optical injection as well [19]-[21], which is beneficial for further suppressing the destructive interference. Employing the dual-mode injection-locking scheme, this work reports an efficient NDFWM generation in a U-band InAs/InP(100) QD FP laser. In the experiment, one tone of the injected continuous-wave (CW) beams is used as the pump wave, while the other one plays the role of the probe wave. Each of these locks a longitudinal mode of the FP laser within the stable-locking range.

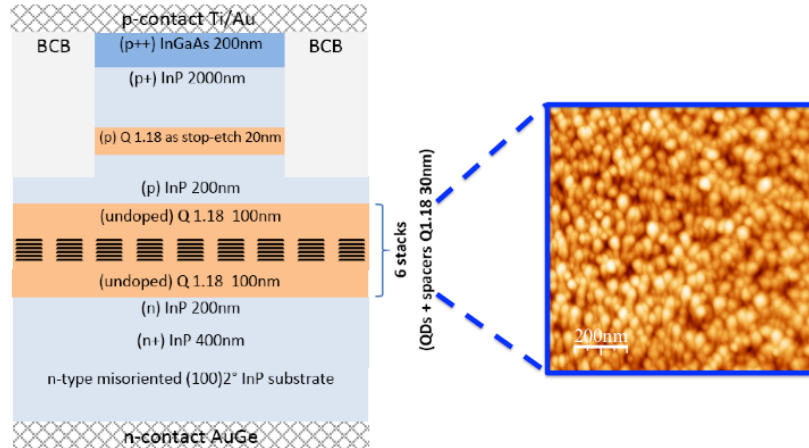


Fig. 1. The epi-layer structure of the InAs/InP(100) QD laser. “Q1.18” denotes that the quaternary alloy In_{0.8}Ga_{0.2}As_{0.435}P_{0.565} emits at 1.18 μm. The stop-etch layer is used to control the etch depth. ‘BCB’ denotes benzocyclobutene, and ‘+’ or ‘++’ indicates the doping level; Enlarged figure is an AFM picture of the semiconductor nanostructures (6 × 10¹⁰ dots/cm⁻²/layer).

2. DESCRIPTION OF THE QUANTUM DOT DEVICE

Figure 1 illustrates the epi-layer structure of the QD laser under study. The QD structure was grown by gas source molecular beam epitaxy (GSMBE) on a 2° misoriented (100) n-doped InP substrate. The optical polarization ratio estimated from the photoluminescence signal was found to be about 11%. In comparison with conventional quantum dashes (QDashes) for which the polarization ratio is usually about 30%, this result is a clear indication of the presence of true QDs. Consequently, the misorientation allows the formation of QDs instead of QDashes which are traditionally formed on InP(100) oriented substrate [22]. The active layer of the diode laser consists of six stacked layers of InAs dots, which are embedded in an InGaAsP quaternary alloy. Figure 1 shows an enlarged atomic force microscope (AFM) picture of the induced self-assembled nanostructures. Dot dimensions (diameter × height) are 36 nm × 2 nm for a total density per layer of about 6 × 10¹⁰ dots/cm⁻². The 4-μm wide ridge waveguide was fabricated by selective wet and dry etching sequence based on a CH₄-H₂-Ar RIE plasma using a Ti-Au mask. Then, a benzocyclobutene (BCB) layer was spin-coated to planarize the mesa structure and dry-etched back to expose the top surface of the ridge. This self-alignment step enables the p-contact electrode to be defined by Ti-Au e-beam evaporation. The substrate was thinned to 150 μm and a backside n-type metallization was performed with an AuGe sputtered alloy. Finally, the device was cleaved into a 830-μm long cavity.

Figure 2 depicts the room temperature light-current characteristics at room temperature of the solitary QD laser. The output power emitted from the front facet is coupled into a lensed optical fiber. The laser exhibits a threshold current of about 64 mA. Interestingly, when the current increases above threshold, the free-running optical spectrum is broadened as shown in the inset at 90 mA (pink) with a peak centered around 1635 nm, and then splits into two separated peaks. As an illustration, the spectral difference between the split peaks at 110 mA (blue) is 17 nm while it increases up to 23 nm at 160 mA (not shown). The corresponding physical mechanism was attributed to the Rabi oscillation as well as to the state filling effect [23], [24]. It is noted that this typical feature observed in the optical spectrum does not result from the

vertical electronic coupling of the QD multi-layers [25] or from the separate excited state emission [26]. Such a wide split in the optical spectrum provides the possibility for the efficient generation of NDFWM with a wide tuning range.

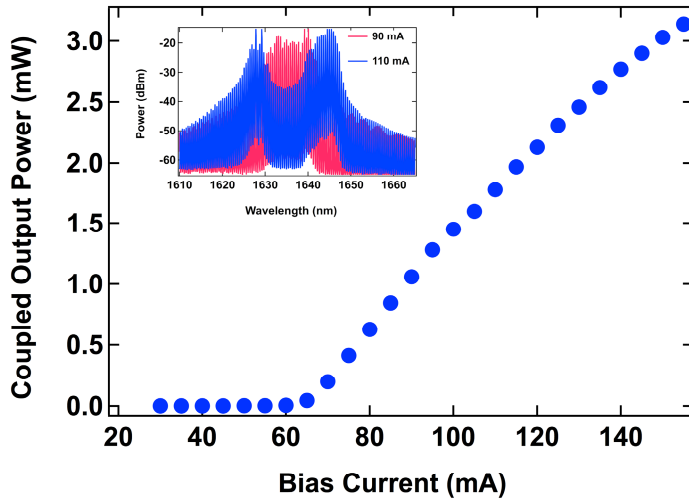


Fig. 2. The room temperature light-current characteristics of the InAs/InP(100) QD laser. The inset shows the free-running spectra measured at 90 mA (pink) and 110 mA (blue). The resolution of the OSA is set at 70 pm.

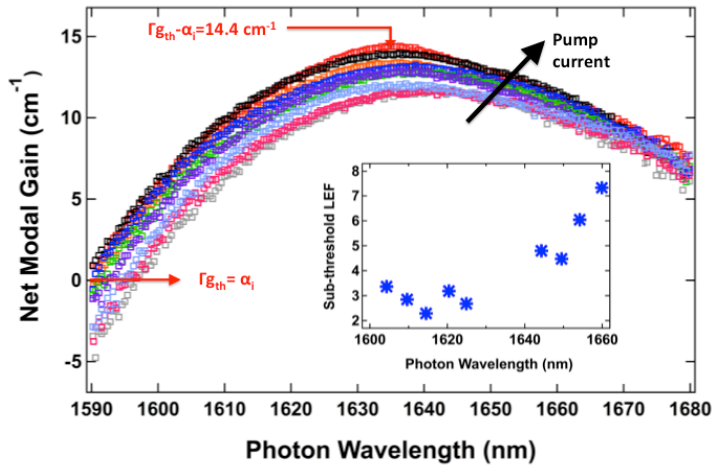


Fig. 3. Sub-threshold net modal gain spectra for different pump currents. The resolution of the OSA is set at 70 pm. The inset shows the measured sub-threshold LEF as a function of the photon wavelength.

Since the LEF has significant influence on the destructive interference effect in the generation of FWM signal. We firstly investigated the LEF of the QD laser device slightly below threshold. By a small change of the pump current ΔI , the LEF (α_H) is defined as the carrier-induced frequency variation $\Delta\omega$ divided by the gain variation Δg [27]:

$$\alpha_H = \frac{2}{v_g} \frac{\Delta\omega / \Delta I}{\Delta g / \Delta I} \quad (1)$$

with v_g the group velocity of the light. Through the amplified spontaneous emission spectrum (ASE), the frequency shift can be directly measured from the optical spectrum analyzer. To remove the thermal red-shift impact on the wavelength, the current injection is operated in the pulsed mode with a pulse width of 10 μs and a duty cycle of 10%. The net modal gain can be extracted from the well-established Hakki-Paoli method [28]. As shown in figure 3, the measured gain spectra were taken between 56 and 63 mA in steps of 0.5 mA. At threshold, the gain spectrum exhibits a full-width at half maximum (FWHM) of about 81 nm and a maximum net modal gain $\Gamma g - \alpha_i$ (where α_i is the internal loss

coefficient) of 14.4 cm^{-1} at 1634.5 nm , the sub-threshold LEF as a function of the wavelength is shown in the inset of figure 3. The LEF value varies from 3.3 to 7.3 over the entire explored U-band (1605 nm - 1660 nm) with a minimum value of 2.6 around $\lambda = 1625 \text{ nm}$. The non-zero LEF value originates from the inhomogeneous broadening as well as the carrier filling in the off-resonant states, which leads to the asymmetric gain spectrum [29], [30]. Although the differential gain is usually strongly reduced at longer wavelengths, the extracted LEF values are relatively similar to those measured on 1520 nm InAs/InP(311B) QD lasers [31].

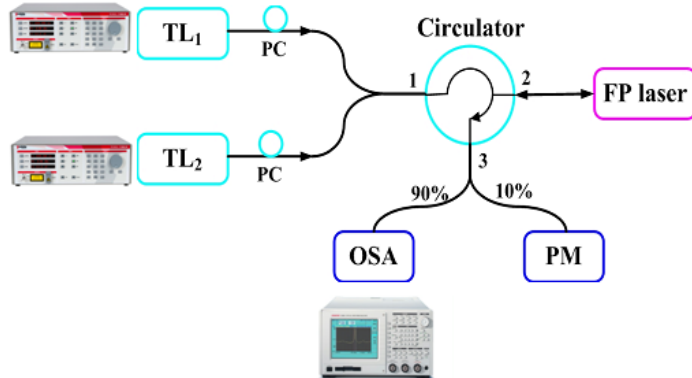


Fig. 4. Schematic of the dual injection-locking experimental setup

3. DUAL OPTICAL INJECTION EXPERIMENTS

Figure 4 shows the experimental setup, where two tunable CW lasers ($\text{TL}_{1,2}$: Yenista Optics, T100S) are injected into the QD laser via an optical circulator. The QD laser output is collected from port 3 of the circulator, which is followed by a 90/10-fiber splitter. The 10% port is connected with a power meter (PM) to monitor the output power while the 90% port is used to analyze the optical spectrum with an optical spectrum analyzer (OSA). The polarization of the tunable lasers is controlled to align with the slave laser through the polarization controller (PC). In the experimental study, the QD laser is biased at 110 mA with a fiber-coupled power of 2.0 mW . Each of the two tunable lasers is set at the maximum achievable power around 1.40 mW (1.43 mW for TL_1 and 1.38 mW TL_2), which are measured at port 2 of the circulator. Assuming a power coupling efficiency of 60% [32], the injection ratio for each of the master lasers to the slave laser is calculated to be 0.42, meaning that the strength of the optical injection remains at a relatively low level. The wavelength of the master laser TL_1 , which is fixed around the center of the peak located at shorter wavelengths acts as the pump wave, while TL_2 is tuned to a longer wavelength and acts as the probe wave.

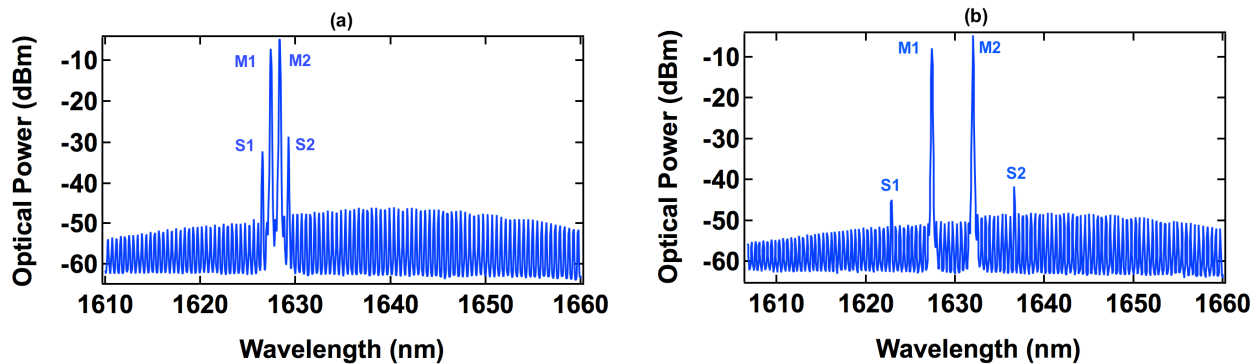


Fig. 5. FWM Optical spectra where $M_{1,2}$ are the stably locked modes by the tunable master lasers. The frequency difference between the locked modes is 109.6 GHz (a) and 528.1 GHz (b). S_1 and S_2 are generated as the converted conjugate signal of M_2 and M_1 .

Figure 5 shows two optical spectra of the dual-mode injection-locked QD laser. Each injected wavelength selects a longitudinal mode within the free-running FP multimodes, while all other modes are well suppressed. M_1 and M_2 are the stable locked modes by TL_1 and TL_2 , respectively. Due to the third-order nonlinear susceptibility $\chi^{(3)}$, new waves S_1 and

S_2 are generated as the converted conjugate signal of M_2 and M_1 . Assuming the frequency difference between M_1 and M_2 is $\Delta f = f_{M1} - f_{M2}$, the FWM process is governed by the carrier density pulsation (CDP) mechanism for Δf within a few GHz [33], where the beating between the pump and probe waves creates temporal gain and index gratings. For larger frequency detunings up to THz range, spectral hole burning (SHB) and carrier heating (CH) dominates. In the SHB mechanism, the injected signals create a hole and change the intraband carrier distribution, producing a modulation of the occupation probability of carriers within the energy band [34]. In the case of QD lasers, the slow interdot processes on the order of a few to tens of picoseconds allow for the creation of deeper spectral holes and thus for more efficient FWM [11]. The CH mechanism is caused by the stimulated emission from the ground state, which removes the lowest energy carriers, while free carriers absorb photons and increase the energy [11], [34]. The frequencies of the two newly generated signals respectively are $f_{S1} = f_{M1} + \Delta f$ and $f_{S2} = f_{M2} - \Delta f$. As an illustration, figure 5(a) shows the occurrence of the FWM effect with a frequency difference of 109.6 GHz while the latter increases up to 528.1GHz in figure 5(b).

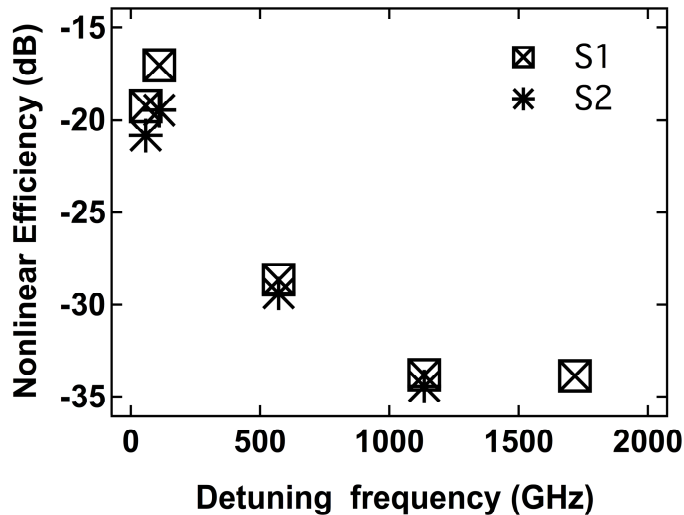


Fig. 6. The normalized conversion efficiency (NCE) for the newly converted signals S_1 , S_2 as a function of the detuning frequency. Note that signal S_2 at 1.72 THz is invisible because it is submerged in the residual FP modes.

The normalized conversion efficiency (NCE) for each converted signal (S_1 , S_2) can be calculated as follows [35]:

$$\eta_{S1} = \frac{P_{S1}}{P_{M1}^2 P_{M2}} \quad (2)$$

$$\eta_{S2} = \frac{P_{S2}}{P_{M2}^2 P_{M1}}$$

where P_X ($X=M_{1,2}$, $S_{1,2}$) is the corresponding wave power, which can be extracted from the optical spectrum. Following this definition, the NCE of the newly converted signals S_1 , S_2 in the QD laser is presented in figure 6 as a function of the detuning frequency. The detuning frequency is operated from the minimum 57.6 GHz up to the maximum 1.72 THz. For even larger detunings up to 5.7 THz, the FWM signal is submerged in the residual FP modes or noise and disappears. Representing the susceptibilities $\chi_{CDP}^{(3)}$, $\chi_{SHB}^{(3)}$ and $\chi_{CH}^{(3)}$ as complex phasors [14], it is found that this finite LEF value causes the phasors to be oriented in different directions at zero detuning. When the frequency difference is tuned, on one hand $\chi_{CDP}^{(3)}$ begins to rotate and its direction becomes closer to that of $\chi_{SHB}^{(3)}$ and $\chi_{CH}^{(3)}$. On the other hand, because the magnitude of each susceptibility becomes smaller, η increases and reaches the peak value when the three additive susceptibilities is at the largest. In the experiment under study, this situation is achieved at the detuning frequency $\Delta f=109.6$ GHz with a normalized conversion efficiency of -17 dB (η_{S1}). Beyond that, the direction of $\chi_{CDP}^{(3)}$ deviates away and the conversion efficiency decreases with the detuning frequency. When Δf is tuned above the characteristic rates (1 THz) of the SHB and CH processes, $\chi_{SHB}^{(3)}$ and $\chi_{CH}^{(3)}$ also begin to rotate making η nearly constant at about -34 dB from $\Delta f=1.13$ THz to 1.72 THz in the experiment. It is noted that at a detuning frequency around 1.1 THz, the NCE of

the studied QD laser is more than 15 dB larger than that of a QW SOA reported in [35]. The experimental results depicted in figure 6 also show that η_{S2} remains slightly smaller than η_{S1} , which is attributed to the assertion that the SHB effect contributes less to the wavelength up-conversion [36]. In addition, figure 7 exhibits the SMSR for the newly converted signals S₁, S₂ as a function of the detuning frequency. The SMSR decreases with the detuning frequency and the highest ratio is 20.3 dB at $\Delta f = 109.6$ GHz. The SMSR of S₂ is smaller in comparison with S₁, which can be partly attributed to the lower power of S₂. On the other hand, the amplitude of the residual FP modes at the longer wavelength side is higher when the laser is injection locked. This phenomenon is because the gain at the right side of the pump wave M₁ is larger than that at the left side.

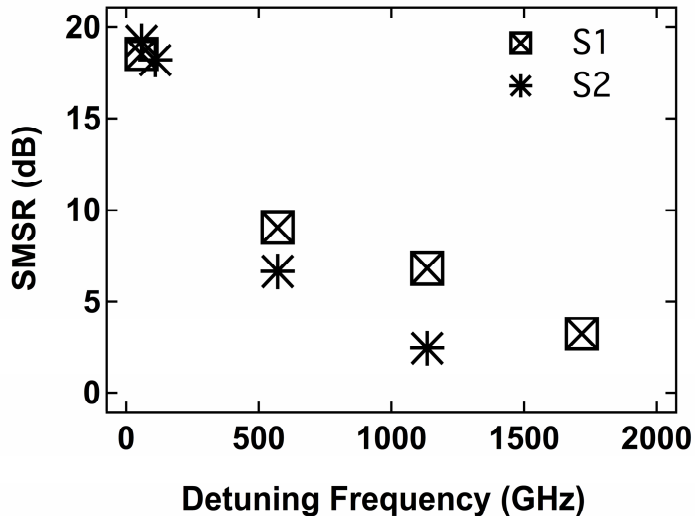


Fig. 7. The SMSR as a function of the detuning frequency for the newly converted signals S₁, S₂ as a function of the detuning frequency. Note that signal S₂ at 1.72 THz is invisible because it is submerged in the residual FP modes.

Last but not least, it is important to note that in the experiment both the pump wave and the probe signal are operated in the stable-locked regime. However, for an arbitrary probe wavelength the temperature of the FP laser can be controlled to tune one of the FP modes within the stable-locking range of the probe signal. In addition, because the converted signal is enhanced by the cavity resonance, it is important to make the converted signal coincide with one of the resonance frequency peaks in the laser cavity [37]. This can be achieved by tuning the pump wave since it typically has a large power and thus a wide locking range. Furthermore, the NCE can be enhanced by a larger bias current to the FP laser, since the output power is mainly determined by the slave laser. The SMSR can be improved by a higher injection ratio [37], which can be achieved by coupling an amplifier into the configuration to amplify the pump wave power. Unfortunately, the impact of the injection strength on the FWM was not studied in this work due to the power limitation of the devices, which will be fulfilled in a following study.

4. CONCLUSIONS

In conclusion, we have experimentally investigated the NDFWM in a U-band QD FP laser employing the dual-mode injection-locking technique. Taking advantage of the two-peak lasing features of the free-running laser arising from the Rabi oscillation, an efficient NDFWM is demonstrated with a tuning range from 58 GHz up to 1.7 THz under a weak optical injection level. The overall performance can be further enhanced by increasing the FP laser bias current and by a higher injection ratio of the pump wave, which will require further investigation in the future. These results are of prime importance for the wavelength conversion technique in high-speed WDM systems as well as for microwave and terahertz signal generations.

ACKNOWLEDGMENTS

The authors would like to thank Professor Alain Le Corre from INSA-Rennes for providing the QD materials. Dr. Frédéric Grillot's work is supported by the European Office of Aerospace Research and Development (EOARD) under grant number FA8655-12-1-2093. Cheng Wang's work is supported by China Scholarship Council.

REFERENCES

- [1] Tatham, M. C., Sherlock, G. and Westbrook, L. D., "20-nm optical wavelength conversion using nondegenerate four-wave mixing," *IEEE Phonon. Technol. Lett.* 5(11), 1303-1306 (1993).
- [2] Geraghty, D. F., Lee, R. B., Verdiell, M., Ziari, M., Mathur, A. and Vahala, K. J., "Wavelength conversion for WDM communication systems using four-wave mixing in semiconductor optical amplifiers," *IEEE J. Sel. Top. Quantum Electron.* 3(5), 1146-1155 (1997).
- [3] Tatham, M. C., Gu, X., Westbrook, L. D., Sherlock, G. and Spirit, D. M., "Transmission of 10 Gbit/s directly modulated DFB signals over 200 km standard fibre using mid-span spectral inversion," *Electron. Lett.* 30(16), 1335-1336 (1994).
- [4] Marcenac, D. D., Nesson, D., Kelly, A. E., Brierly, M., Elllis, A. D., Moodie, D. G. and Ford, C. W., "40 Gbit/s transmission over 406 km of NDSF using mid-span spectral inversion by four-wave mixing in a 2 mm long semiconductor optical amplifier," *Electron. Lett.* 33(10), 879-880 (1997).
- [5] Kim, H. J., Song, H. J. and Song, J. I., "All-optical frequency up-conversion technique using four-wave mixing in semiconductor optical amplifiers for radio-over-fiber applications," *Microwave Symposium. IEEE/MTT-S International*, 67-70 (2007).
- [6] D'Ottavi, A., Martelli, F., Spano, P., Mecozzi, A., Scotti, S., D'Ara, R., Eckner, J. and Guekos, G., "Very high efficiency four-wave mixing in a single semiconductor traveling wave amplifier," *Appl. Phys. Lett.*, 68(16), 2186-2188 (1996).
- [7] Simoyama, T., Kuwatsuka, H. and Ishikawa, H., "Cavity length dependence of wavelength conversion efficiency of four-wave mixing in $\lambda/4$ -shifted DFB laser," *FUJISU Sci. Tech. J.* 34(2), 235-244 (1998).
- [8] Kim, H. J. and Song, J. I., "All-optical frequency down conversion technique utilizing a four-wave mixing effect in a single semiconductor optical amplifier for wavelength division multiplexing radio-over-fiber applications," *Optics Express* 20(7), 8047-8054 (2012).
- [9] Su, H., Li, H., Zhang, L., Zou A. L. Gray, Z., Wang, R., Varangis, P. M. and Lester, L. F., "Nondegenerate four-wave mixing in quantum dot distributed feedback lasers," *IEEE Phonon. Technol. Lett.* 17(8), 1686-1688 (2005).
- [10] Li, H., Liu, G. T., Varangis, P. M., Newell, T. C., Stintz, A., Fuchs, B., Malloy, K. J. and Lester, L. F., "150-nm tuning range in a grating-coupled external cavity quantum-dot laser," *IEEE Photon. Technol. Lett.* 12(7), 759-761 (2000).
- [11] Nielsen, D. and Chuang, S. L., "Four-wave mixing and wavelength conversion in quantum dots," *Phys. Rev. B* 81(3), 035305 (2010).
- [12] Akiyama, T., Wada, O., Kuwatsuka, H., Simoyama, T., Nakata, Y., Mukai, K., Sugawara, M. and Ishikawa, H., "Nonlinear processes responsible for nondegenerate four-wave mixing in quantum-dot optical amplifiers," *Appl. Phys. Lett.* 77(12), 1753-1755 (2000).
- [13] Lu, Z. G., Liu, J. R., Raymond, S., Poole, P. J., Barrios, P. J., Poitras, D., Sun, F. G., Pakulski, G., Bock, P. J. and Hall, T., "Highly efficient non-degenerate four-wave mixing process in InAs/InGaAsP quantum dots," *Electron. Lett.* 42(19), 1112-1113 (2006).
- [14] Akiyama, T., Kuwatsuka, H., Hatori, N., Nakata, Y., Ebe, H. and Sugawara, M., "Symmetric highly efficient (~ 0 dB) wavelength conversion based on four-wave mixing in quantum dot optical amplifiers," *IEEE Phonon. Technol. Lett.* 14(8), 1139-1141 (2002).
- [15] Flayyih, A. H. and Al-Khursan, A. H., "Four-wave mixing in quantum dot semiconductor optical amplifiers," *Applied Optics* 52(14), 3156-3165 (2013).
- [16] Yabre, G., "Effect of relatively strong light injection on the chirp-to-power ratio and the 3 dB bandwidth of directly modulated semiconductor lasers," *J. Lightwave Tech.* 14, 2367-2373 (1996).
- [17] Simpson, T. B., Liu, J. M. and Gavrielides, A., "Bandwidth enhancement and broadband noise reduction in injection-locked semiconductor lasers," *IEEE Phonon. Technol. Lett.* 7(7), 709-711 (1995).
- [18] Meng, X. J., Chau, T. and Wu, M. C., "Improved intrinsic dynamic distortions in directly modulated semiconductor lasers by optical injection locking," *IEEE Trans. Microw. Theory Tech.* 47 (7), 1172-1176 (1999).
- [19] Naderi, N. A., Pochet, M. C., Grillot, F., Shirkhorshidian, A., Kovanis, V. and Lester, L. F., "Manipulation of the linewidth enhancement factor in an injection-locked quantum-dash Fabry-Perot laser at 1550 nm," *23rd Annual Meeting of the IEEE Photonics Society*, 427-428 (2010).

- [20] Lingnau, B., Ludge, K., Chow, W. W. and Scholl, E., "Failure of the α factor in describing dynamical instabilities and chaos in quantum-dot lasers" Phys. Rev. E 86(6), 065201 (2012).
- [21] Lin, C. H., and Lin, F. Y., "Four-wave mixing analysis on injection-locked quantum dot semiconductor lasers," Opt. Express 21(18), 21242-21253 (2013).
- [22] Lelarge, F., Dagens, B., Renaudier, J., Brenot, R., Accard, A., Van Dijk, F., Make, D., Le Gouezigou, O., Provost, J. G., Poingt, F., Landreau, J., ; Drisse, O., Derouin, E., Rousseau, B., Pommereau, F. and Guang-Hua Duan, G. H., "Semiconductor lasers and optical amplifiers operating at 1.55 μm ," IEEE J. Sel. Top. Quantum. Electron. 13(1), 111-124 (2007).
- [23] Li, S. G., Gong, Q., Lao, Y. F., Yang, H. D., Gao, S., Chen, P., Zhang, Y. G., Feng, S. L. and Wang, H. L., "Two-color quantum dot laser with tunable wavelength gap," Appl. Phys. Lett. 95(25), 251111-251113 (2009).
- [24] Stievater, T. H., Li, X. Q., Steel, D. G., Gammon, D., Katzer, D. S., Park, D., Piermarocchi, C. and Sham, L. J., "Rabi oscillations of excitons in single quantum dots," Phys. Rev. Lett. 87(13), 133603-133606 (2001).
- [25] Miska, P., Even, J., Paranthoen, C., Dehaese, O., Jbeli, A., Senès, M. and Marie, X., "Vertical electronic coupling between InAs/InP quantum-dot layers emitting in the near-infrared range," Appl. Phys. Lett. 86(11), 111905-111907 (2005).
- [26] Cornet, C., Schliwa, A., Even, J., Doré, F., Celebi, C., Létoublon, A., Macé, E., Paranthöen, C., Simon, A., Koenraad, P. M., Bertru, N., Bimberg, D. and Loualiche, S., "Electronic and optical properties of InAs/InP quantum dots on InP(100) and InP(311)B substrates: Theory and experiment," Phys. Rev. B 74(3), 3035312 (2006).
- [27] Provost, J. G. and Grillot, F., "Measuring the Chirp and the Linewidth Enhancement Factor of Optoelectronic Devices with a Mach-Zehnder Interferometer," IEEE Photonics Journal 3(3), 476-488 (2011).
- [28] Raghuraman, R., Yu, N., Engelmann, R., Lee, H. and Shieh, C. L., "Spectral dependence of differential gain, mode shift, and linewidth enhancement factor in a InGaAs-GaAs strained-layer single-quantum-well laser operated under high-injection conditions," IEEE J. Quantum. Electron. 29(1), 69-75 (1993).
- [29] Grillot, F., Dagens, B., Provost, J. G., Su, H. and Lester, L. F., "Gain compression and above-threshold linewidth enhancement factor in 1.3 μm InAs-GaAs quantum-dot lasers," IEEE J. Quantum. Electron. 44(10), 946-951 (2008).
- [30] Gioannini, M., Sevega, A. and Montrosset, I., "Simulations of differential gain and linewidth enhancement factor of quantum dot semiconductor lasers," Opt. Quantum Electron. 38(4-6), 381-394 (2006).
- [31] Martinez, A., Merghem, K., Bouchoule, S., Moreau, G., Ramdane, A., Provost, J. G., Alexandre, F., Grillot, F., Dehaese, O., Piron, R. and Loualiche, S., "Dynamic properties of InAs/InP(311B) quantum dot Fabry-Perot lasers emitting at 1.52- μm ," Appl. Phys. Lett. 93(2), 021101 (2008).
- [32] Naderi, N. A., Pochet, M., Grillot, F., Terry, N. B., Kovanis, V. and Lester, L. F., "Modeling the injection-locked behavior of a quantum dash semiconductor laser," IEEE J. Sel. Top. Quantum. Electron. 15(3), 563-571 (2009).
- [33] Agrawal, G. P., "Population pulsations and nondegenerate four-wave mixing in semiconductor lasers and amplifiers," J. Opt. Soc. Am. B 5(1), 147-159 (1988).
- [34] Kikuchi, K., Kakui, M., Zah, C. E. and Lee, T. P., "Observation of highly nondegenerate four-wave mixing in 1.5 μm traveling-wave semiconductor optical amplifiers and estimation of nonlinear gain coefficient," IEEE J. Quantum. Electron. 28(1), 151-156 (1992).
- [35] Koltchanov, I., Kindt, S., Petermann, K., Diez, S., Ludwig, R., Schnabel, R. and Weber, H. G., "Analytical theory of terahertz four-wave mixing in semiconductor-laser amplifiers," Appl. Phys. Lett. 68(20), 2787-2789 (1996).
- [36] D'Ottavi, A., Iannone, E., Mecozzi, A., Scotti, S., Spano, P., Landreau, J., Ougazzaden, A. and Bouley, J. C., "Investigation of carrier heating and spectral hole burning in semiconductor amplifiers by highly nondegenerate four-wave mixing," Appl. Phys. Lett. 64(19), 2492-2494 (1994).
- [37] Li, L. L. and Petermann, K., "Small-signal analysis of THz optical-frequency conversion in an injection-locked," IEEE J. Quantum. Electron. 29(12), 2988-2994 (1993).